Available online at www.sciencedirect.com
ScienceDirect
Journal of Natural Gas Chemistry 19(2010)333–340
Journal of Natural Gas Chemistry
www.elsevier.com/locate/jngc

Deactivation studies of nano-structured iron catalyst in Fischer-Tropsch synthesis

Ali Nakhaei Pour[1,2*], Mohammad Reza Housaindokht[1], Sayyed Faramarz Tayyari[1], Jamshid Zarkesh[2]

1. Department of Chemistry, Ferdowsi University of Mashhad, P. O. Box 91775-1436, Mashhad, Iran;
2. Research Institute of Petroleum Industry of National Iranian Oil Company, P. O. Box 14665-137, Tehran, Iran

[Manuscript received September 11, 2009; revised October 15, 2009]

Abstract

A nano-structured iron catalyst for syngas conversion to hydrocarbons in Fischer-Tropsch synthesis (FTS) was prepared by micro-emulsion method. Compositions of bulk iron phase and phase transformations of carbonaceous species during catalyst deactivation in FTS reaction were characterized by temperature-programmed surface reaction with hydrogen (TPSR-H_2), and XRD techniques. Many carbonaceous species on surface and bulk of the nano-structured iron catalysts were completely identified by combined TPSR-H_2 and XRD spectra and which were compared with those recorded on conventional co-precipitated iron catalyst. The results reveal that the catalyst deactivation results from the formation of inactive carbide phases and surface carbonaceous species like graphite, and it will be increased when the particle size of iron oxides was reduced in FTS iron catalyst.

Key words

Fischer-Tropsch synthesis; iron-based catalyst; catalyst deactivation; nano-size particles

1. Introduction

The Fischer-Tropsch synthesis (FTS) offers the possibility of converting a mixture of hydrogen and carbon monoxide (syngas) into clean hydrocarbons, free from sulfur [1−4]. Iron-based catalysts are preferred for FTS utilizing synthesis gas derived from coal or biomass because of the excellent activity for the water-gas-shift reaction, which allows using a synthesis gas with a low H_2/CO ratio directly without an upstream shift-step. But it is well known that low product selectivity, catalyst agglomeration and sintering limit the use of iron catalysts in high temperate operation [5−8]. It is important in design of iron-based FT catalysts to achieve a clear understanding of carbon species deposition and phase-transformation of iron catalyst during different pretreatments and under industrial FTS conditions. Results of previous studies have shown that the formation of surface carbides is required before the catalyst can exhibit high activity [9−11]. However, the correlation among bulk carbide species, surface carbon species, and catalytic activity has not yet been established. It is well known that the distribution of iron phases in the catalyst changes during time on stream [12,13]. Although the active phase for the FTS reaction is still in debate, the oxidation of the metallic iron and/or the iron carbide phases is believed as one of the factors for catalyst deactivation. H_2O (the primary product in the FTS reaction) and CO_2 (produced from water-gas shift reaction) are usually considered as the oxidizing agents for iron phases [14,15]. Apart from the oxidation of the iron phases, several authors have pointed out the importance of a graphite-like carbonaceous compound on the deactivation of the iron catalysts [16−18].

Xu and Bartholomew [19] identified and quantified several carbon and metal carbide species on the surface of unsupported and supported used iron catalysts by means of temperature-programmed surface reaction with hydrogen (TPSR-H_2). In both systems, good correlation between coverage of atomic surface carbon species and catalyst performance was found. Herranz et al. [13] studied the effect of pretreatment condition on active phase formation during the activation of iron catalyst. They reported that only metallic iron was formed when the pretreatment is performed with hydrogen. However, iron carbide, mainly cementite and the Hägg carbide are formed with CO (pure or diluted) and/or syngas pretreatments. In our previous work, the effects of Ca, Mg and La promoters on the activity and products selectivity of iron catalysts were studied during FTS performance [20,21]. These results showed that the catalyst deactivation is increased with increasing the catalyst surface basicity via formation of

* Corresponding author. Tel/Fax: +98 21 44739716; Email: nakhaeipoura@ripi.ir and nakhaeipoura@yahoo.com

doi:10.1016/S1003-9953(09)60061-X

inactive carbon (graphitic) and less active iron carbide (cementite). Recent studies showed that nano-sized iron particles played an essential role to achieve high FTS activity [22−27]. In the last years, it has been generalized the use of microemulsions for the synthesis of nanoparticles with controlled size displaying a homogeneous distribution of both elements throughout the solid [24,25]. A prepared microemulsion catalyst, which is optically transparent and has thermodynamically stable dispersion of water phase into an organic phase, is stabilized by a surfactant [26]. The different species (oxide precursors) are homogeneously mixed within the micelles, therefore rendering the solids displayed high internal homogeneity and optimal interaction between the constituents [24,25]. Some authors, prepared supported iron-based Fischer-Tropsch catalysts by microemulsion, reported high activity and marked selectivity to oxygenates. In our previous works, the effects of nano-size iron particles on catalyst structure, surface area, reduction and carburization, textural properties, and activity behavior of precipitated Fe/Cu/La catalyst in a fixed bed reactor have been studied [28,29].

Consequently, a detailed characterization study of the nature of the bulk and surface species formed in nano-size iron particles during FTS reaction was performed in the present work. Effects of nano-size iron particles in carbonaceous species were studied on the surface of the iron catalysts by XRD and temperature-programmed surface reaction with hydrogen (TPSR-H_2) after pretreatment and FTS reaction. The characterization results were correlated with the catalytic activity measurements.

2. Experimental

2.1. Catalyst preparation

The Fe/Cu/La conventional catalyst was prepared by co-precipitation of Fe and Cu nitrates at a constant pH to form porous Fe-Cu oxyhydroxide powders that were promoted by impregnation with $La(NO_3)_3$ precursor after treatment in air as described previously [20].

The Fe/Cu/La nanostructure catalyst was prepared by co-precipitation in a water-in-oil microemulsion. A water solution of metal precursors, $Fe(NO_3)_3{\cdot}9H_2O$ (Fluka, >98%) and/or $Cu(NO_3)_2{\cdot}4H_2O$ (Fluka, purum, >97%) was added to a mixture of an oil phase containing 1-butanol (Aldrich, >99%) and chloroform (Aldrich, >99%) with a ratio of 60 to 40 and sodium dodecyl sulfate (SDS) as surfactant was added to a solution. The obtained mixture had the following composition: 10 wt.% of aqueous phase, 70 wt.% of oil phase and 20 wt.% of surfactant. After stirring, a transparent mixture, which was stable for at least 24 h was obtained. A similar microemulsion containing NH_4OH (28.0%–30.0%) in the aqueous phase was used as the precipitating agent. The obtained mixture was left to decant overnight. The solid was recovered by centrifugation and washed thoroughly with distilled water and ethanol. Finally, the samples were dried overnight at 393 K, and subsequently calcined in air at 773 K for 6 h. Lanthanum promoter was added by wetness impregnation. $La(NO_3)_3$ precursor was set to the optimal value after treatment in air as described previously [28]. The promoted catalysts were dried at 383 K for 16 h and calcined at 773 K for 3 h in air. The catalyst compositions were designated in terms of the atomic ratios as: 100Fe/5.64Cu/2La. All samples were pressed into pellets, crushed and sieved to obtain 100−180 μm particles which have been proved to be a compromising particle size safe for neglecting intraparticle transfer limitations and promisingly easy operations to the reactor during the experiment.

2.2. Catalyst characterization

The oxide precursors as well as the catalysts after pretreatment and FTS reaction were characterized by XRD and TPSR-H_2. In our previous work, a complete characterization of catalysts was described [28,29]. X-ray diffraction (XRD) spectra of fresh catalysts were collected with a Philips PW1840 X-ray diffractometer using monochromatized Cu (K_α) radiation to determine catalyst phases after calcinations, pretreatment and FTS reaction. For determining catalyst phases after pretreatment and FTS reaction, the samples were passivated with an 1 vol% O_2/He mixture at room temperature for 1 h according to a standard procedure described elsewhere [13,30]. Then the samples were analyzed by X-ray diffraction (XRD) and different species detected from the XRD analysis according to the JCPDS cards.

For the temperature-programmed surface reaction with hydrogen (TPSR-H_2) ca. 0.5 g of the sample was loaded into a U-shaped quartz reactor. The samples were pretreated in a 5%(v/v) H_2/N_2 gas mixture with space velocity of 15.1 nl·h^{-1}·g$_{Fe}^{-1}$ at 0.1 MPa by increasing temperature from ambient to 673 K with 5 K/min, then maintained for one hour and subsequently reduced to 543 K. The activation was followed by the synthesis gas stream with $H_2/CO = 1$ and space velocity of 3.07 nl·h^{-1}·g$_{Fe}^{-1}$ for 24 h in 0.1 MPa and 543 K and then flushed with Ar at 543 K until the baseline leveled off (ensuring complete removal of adsorbed species on the reduced catalyst surface has been achieved). Then the samples were cooled to room temperature under Ar flow for TPSR-H_2 test. The reactivity of the species remained on the surface of the solids was tested by H_2/Ar (10%) flow. The gas flow rate was 50–100 ml/min, and the temperature was increased from 300 to 1100 K at a linear heating rate of 5 K/min. The outlet of the microreactor passed through a condenser and zeolite trap to remove liquefied phases (especially water), then connected to a Shimadzu 4C gas chromatograph equipped with two subsequently connected packed columns: Porapak Q and Molecular Sieve 5A, and a thermal conductivity detector (TCD) with argon which was used as a carrier gas for hydrogen and CH_4 analysis.

For evaluation of catalysts after FTS reaction, the samples were flushed with Ar at 543 K until the baseline leveled off (ensuring complete removal of adsorbed species on the reduced catalyst surface had been achieved). Then the samples

were cooled to room temperature under Ar flow for (TPSR-H_2) tests. The reactivity of the species remaining on the surface of the solids was tested by passing H_2/Ar (10%). The gas flow rate was 50–100 ml/min, and the temperature was increased from 300 to 1100 K at a linear heating rate of 5 K/min. The outlet of the microreactor passed through a condenser and zeolite trap to remove liquefied phases, then it was connected to a Shimadzu 4C gas chromatograph.

2.3. Catalytic performance

The catalysts were tested in a fixed-bed microreactor. A detailed description of the experimental setup and procedures has been provided elsewhere [20]. The catalyst samples (3.0 g catalyst diluted with 12 g quartz, 100−180 μm) were activated by a 5%(v/v) H_2/N_2 gas mixture with space velocity of 15.1 nl·h^{-1}·g$_{Fe}^{-1}$ at 0.1 MPa by increasing the temperature from ambient to 673 K at 5 K/min, then maintained for one hour, and subsequently reduced to 543 K. The pretreatment was followed by the passage of synthesis gas stream with $H_2/CO = 1$ and space velocity of 3.07 nl·h^{-1}·g$_{Fe}^{-1}$ for 24 h in 0.1 MPa and 543 K before attaining the FTS reaction temperature and pressure. After catalyst pretreatment, synthesis gas was fed to the reactor at 563 K, 17 bar, $(H_2/CO)_{feed} = 1$ and a space velocity of 4.9 nl·h^{-1}·g$_{Fe}^{-1}$.

The products were analyzed by means of three gas chromatographs, a Shimadzu 4C gas chromatograph equipped with two subsequently connected packed columns: Porapak Q and Molecular Sieve 5A, and a thermal conductivity detector (TCD) with argon which was used as a carrier gas for hydrogen analysis. A Varian CP 3800 with a chromosorb column and a thermal conductivity detector (TCD) was used for CO, CO_2, CH_4, and other non-condensable gases. A Varian CP 3800 with a Petrocol^{Tm} DH100 fused silica capillary column and a flame ionization detector (FID) was used for organic liquid products so that a complete product distribution could be provided.

3. Results

3.1. Catalytic activity

The samples were tested in the FTS reaction at 563 K for 105 h. The variation of CO conversion rate (mol/h) with time-on-stream is shown in Figure 1. As shown in this Figure, the CO conversion improves significantly while the catalyst crystal size decreases. Figure 1(a) shows that the nanostructure catalyst has higher catalyst deactivation rate and CO conversion drop in comparison with conventional catalysts. By using power law equation for both catalysts, it is possible to write formulas for deactivation rates of catalysts. As shown in Figure 1(b):

$$X_{CO} = 1.3117t^{-0.511} \quad \text{nano catalyst} \quad (1)$$

$$X_{CO} = 0.7326t^{-0.372} \quad \text{conventional catalyst} \quad (2)$$

Where t is time on stream and X_{CO} is CO conversion rate (mole/h). Assuming that the deactivation rate of catalysts can be written as a general form in order to derive kinetics formula for deactivation rates [8]:

$$-dX_{CO}/dt = KX_{CO}^{n} \quad (3)$$

Where n is the degree of reaction and K is an integral parameter and must be determined for both equations. After integration and calculation, degrees of reaction and integral parameters were determined as follows:

$$-dX_{CO}/dt = 0.30X_{CO}^{2.96} \quad \text{nano catalyst} \quad (4)$$

$$-dX_{CO}/dt = 3.70X_{CO}^{0.86} \quad \text{conventional catalyst} \quad (5)$$

These formulas indicated that the deactivation rate of nano catalyst was higher than the conventional.

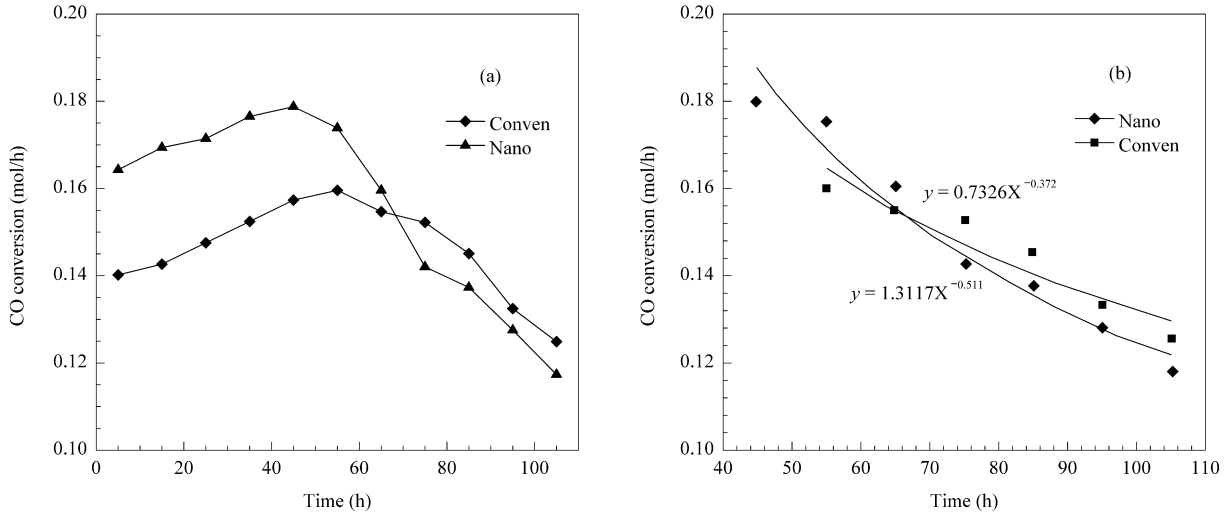

Figure 1. Crystal size effects on CO conversion versus time-on-stream. Reaction conditions: 563 K, $H_2/CO = 1$, 1.7 MPa, SV = 4.9 nl·h^{-1}·g$_{Fe}^{-1}$

Table 1 displays the effect of the catalyst crystal size on catalyst activity, product selectivity and hydrocarbon distribution at the same time on stream. In this Table, the methane selectivity increases when the CO_2 selectivity decreases from conventional to nano catalyst. Selectivity towards higher hydrocarbons shows drop off trend in carbon number from conventional to nano catalyst.

Table 1. Catalyst activity and product selectivity after 52 h

Catalyst	X^{a}_{CO}	HC[b]	O/P[c]	α[d]	CO_2 (%)[e]	Products selectivity			
						CH_4	C_2–C_4	C_5–C_{12}	C_{12+}
Conventional	64.1	24.5	1.1	0.65	34.3	17.2	35.2	29.4	18.2
Nano size	76.5	27.2	1.0	0.61	32.2	18.7	36.8	33.6	10.9

Reaction conditions: 563 K, 1.7 MPa, $H_2/CO = 1$, space velocity = 4.9 nl·h^{-1}·g$_{Fe}^{-1}$;
[a]Carbon monoxide conversion (mol%);
[b]Hydrocarbon production, $g_{CH_2}/(g_{Fe}\cdot s)$ ($\times 10^5$), CH_4 free;
[c]Olefin to paraffin ratio;
[d]Chain growth probability;
[e]CO_2 selectivity. Selectivity to oxygenates was negligible (<2.0%) in all cases

3.2. Crystalline structure exists in fresh catalysts, after pretreatment and after FTS reaction

Nanostructure and conventional iron catalysts characterized by XRD measurements after calcination are shown in Figure 2. The pattern of the conventional and nano-structured catalysts indicate that rhombohedral hematite (Fe_2O_3) with corundum-type structure has characteristic diffraction peaks at 2θ values of 24.3°, 33.3°, 35.8°, 40.8°, 49.6°, 54.1°, 57.6° and 64.1° [31], respectively. The average value of the the crystal size in the nano catalyst was determined to be about 22 nm by using Scherrer equation. Diffraction data indicate that the presence of lanthanum and copper and then subsequent treatment in dried air did not influence the hematite crystalline phases detected by X-ray diffractions in different catalyst preparation methods. It shows that the hematite structure once formed remains stable during subsequent aqueous impregnation and thermal treatment.

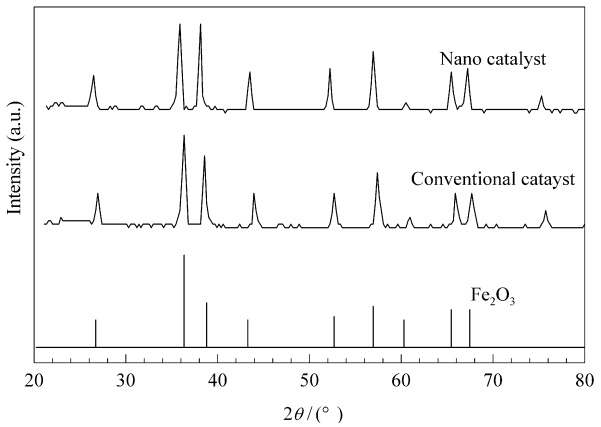

Figure 2. X-ray powder diffraction patterns of the fresh catalysts with different promoters

X-ray powder diffraction patterns (XRD) of the passivated pretreated samples are illustrated in Figure 3. A summary of the different species detected from the XRD analysis (according to the JCPDS card) after the pretreatments is shown in Table 2. Before the XRD analysis, the catalysts were passivated in 1% O_2/He stream at room temperature. As shown in Figure 3, under pretreatment, a broad diffraction peak was observed at ca. 44° in their XRD profiles irrespective of the iron carbides. While the catalyst reduction proceeded, iron oxide was transformed from $Fe_2O_3 \rightarrow Fe_3O_4 \rightarrow$ α-Fe or iron carbide. α-Fe could not be observed in our reduced catalyst because the metallic iron was fairly reactive to dissociated carbon from carbon monoxide. Among the iron carbides, O carbides (carbides with carbon atoms in octahedral interstices, ε-Fe_2C and $\acute{\varepsilon}$-$Fe_{2.2}C$) and TP carbides (carbides with carbon atoms in trigonal prismatic interstices, χ-$Fe_{2.5}C$ and θ-Fe_3C) have been identified [12,13]. The assignment of the different Fe carbide phases ($\acute{\varepsilon}$- $Fe_{2.2}C$, cementite carbide (θ-Fe_3C) and Hägg carbide (χ-$Fe_{2.5}C$)) from the X-ray diffractograms was performed carefully because they showed similar diffraction patterns. According to the JCPDS card, only $\acute{\varepsilon}$- $Fe_{2.2}C$ shows a main diffraction peak near 43° among these carbides [14]. Furthermore, peaks at ca. 39° and 41° were used to identify Hägg carbide (χ-$Fe_{2.5}C$) (JCPDS 36−1248). Peak assignments are based on the characteristic angles of cementite carbide (θ-Fe_3C) (JCPDS 76−1877) at 78.0° and 70.1°, which are not present in the χ-$Fe_{2.5}C$ diffractogram [13]. On the contrary, sharp peaks clearly observed at 35°, 57° and 63° as well in the diffraction profiles are assigned to Fe_3O_4. The relative intensity of the diffraction peaks was taken into account for the identification of the carbide species.

As shown in Figure 3 and Table 2, the nano-catalyst has higher amounts of carbon-rich $\acute{\varepsilon}$-carbides than the conventional catalyst that has more iron-rich χ and θ phases. These results are attributed to lower size of iron crystals that increases the chance of contacts between carbon monoxide and the bulk iron in pretreatments of catalysts and converts bulk iron to more carbon rich $\acute{\varepsilon}$-$Fe_{2.2}C$ carbides. Previous results suggest that the most catalytic active phase in FTS is $\acute{\varepsilon}$-carbide ($Fe_{2.2}C$). It lasts over long period of reaction, converts into the Hägg carbide (χ-$Fe_{2.5}C$) and subsequently changes into the cementite (θ-Fe_3C) with lower carbon content [8,9,32].

Table 2. Phase detected by XRD after activation pretreatment

Catalyst	Phases detected	Fe-carbides/ Fe_3O_4 ratio	$\acute{\varepsilon}$-$Fe_{2.2}C$/(θ-Fe_3C, χ-$Fe_{2.5}C$) ratio
Conventional	Fe_3O_4, θ-Fe_3C, χ-$Fe_{2.5}C$, $\acute{\varepsilon}$-$Fe_{2.2}C$	2.7	1.3
Nano size	Fe_3O_4, θ-Fe_3C, χ-$Fe_{2.5}C$, $\acute{\varepsilon}$-$Fe_{2.2}C$	3.5	2.1

χ-$Fe_{2.5}C$: Hägg carbide; θ-Fe_3C: cementite carbide; Fe_3O_4: magnetite

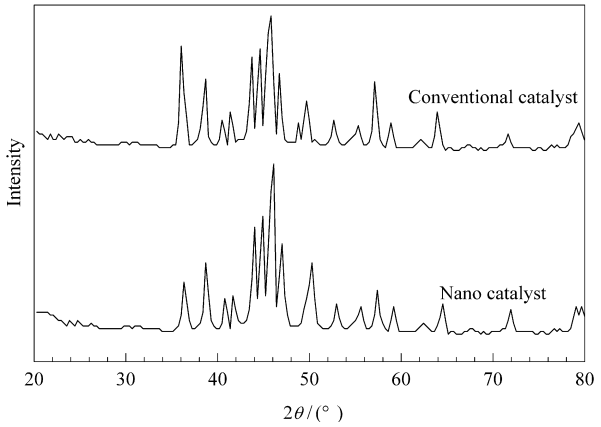

Figure 3. X-ray powder diffraction patterns of the passivated pretreated catalysts with different promoters. Before the measurements, the catalyst was passivated in 1% O_2/He stream at room temperature

Figure 4 shows XRD of conventional and nano-sized iron catalysts after FTS reaction for 105 h. Before the XRD measurements, the catalysts were passivated in 1% O_2/He stream at room temperature. Also, a summary of different species detected from the XRD analysis after FTS reaction is shown in Table 3. The profile of the catalysts after the FTS reaction is quite different due to the difference of catalyst position in the fixed bed reactor. In the fixed bed reactor, the reaction atmosphere changes during the FTS reaction depending on the catalyst position in the reactor because several reactions proceed along with the reactor. At the top of the catalyst bed, the concentration of the feed (CO and H_2) is high but at the down side the product concentration such as hydrocarbons, H_2O and CO_2 increases. Therefore, it is important to investigate iron phases charged in different positions of the reactor in order to clearly show how the catalyst is oxidized during the reaction. From this point of view, we compared iron phases of the catalysts charged at top and on the lower part of the catalyst bed after the reaction. Figure 4 (a) shows XRD profiles of promoted iron catalysts charged at top of the bed after the FTS reaction. As shown in this Figure and Table 3, contrary to the pretreatment results, the nano-catalyst has higher amounts of the cementite carbides (θ-Fe_3C) and magnetite (Fe_3O_4). These results are attributed to higher activity of nano catalyst that increases the concentration of oxidized products (H_2O and CO_2) in reaction atmosphere, converts $\acute{\varepsilon}$-$Fe_{2.2}C$ carbides into the Hägg carbide (χ-$Fe_{2.5}C$) and subsequently transforms into the cementite (θ-Fe_3C) with lower carbon content and magnetite (Fe_3O_4) [6−8]. Therefore, the oxidation of the Fe carbides by H_2O (the primary product in the FTS reaction) and CO_2 (produced via water-gas shift reaction) is more significant on these catalysts. On the other hand, only the diffraction peaks assigned to Fe_3O_4 are observed in the profiles of the catalysts loaded in the lower part of the bed. Although some iron carbide was shown in conventional catalyst after reaction in the samples from bottom of the reactor.

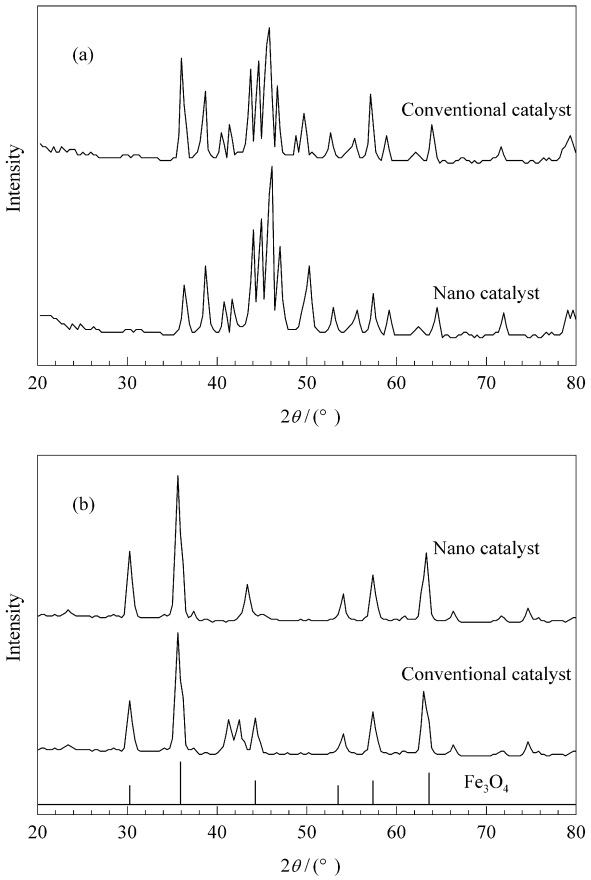

Figure 4. X-ray powder diffraction profiles of iron catalysts after the FTS reaction. (a) Samples located on the top of the catalyst bed in the fixed bed reactor, (b) Samples located on downward of the catalyst bed in the fixed bed reactor

Table 3. Phase detected by XRD for catalysts located at the top of bed after 105 h FTS reaction

Catalyst	Phases detected	Fe-carbides/ Fe_3O_4 ratio	θ-Fe_3C/ χ-$Fe_{2.5}C$ ratio
Conventional	Fe_3O_4, θ-Fe_3C, χ-$Fe_{2.5}C$	5.5	2.3
Nano size	Fe_3O_4, θ-Fe_3C, χ-$Fe_{2.5}C$	3.6	3.4

χ-$Fe_{2.5}C$: Hägg carbide; θ-Fe_3C: cementite carbide; Fe_3O_4: magnetite

3.3. Temperature-programmed surface reaction of catalysts after pretreatment and reaction

Surface carbonaceous species in Fe/Cu/La conventional and nano-structure catalysts were studied by temperature-programmed surface reaction with hydrogen (TPSR-H_2) after pretreatment. A method for qualitative and quantitative analysis of overlapping TPSR-H_2 peaks for iron-based FT catalyst

was reported by Bartholomew et al. [6,19]. TPSR-H_2 spectra, which shows methane evolution rate (due to reaction of carbon with H_2), are plotted in Figure 5 for the samples. The spectra were deconvoluted and fitted with Gaussian curves to yield up to four peaks. Designated as α, β, γ_1, and γ_2, these species are assigned to atomic carbon (carbidic), amorphous surface methyl chains or films, and bulk iron carbides respectively. Peak temperatures increase in order of decreasing reactivity with H_2, and assignments for the species are based on previous literature [13,19].

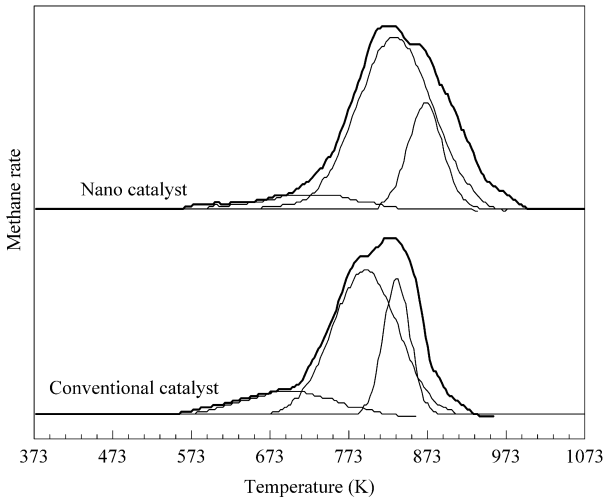

Figure 5. Temperature-programmed surface reaction with hydrogen (TPSR-H_2) of samples after pretreatment

Table 4 shows the peak temperatures and the corresponding percentage compositions of carbon species. The carbon equivalents for α-carbon (the most reactive carbon form), β-carbons and carbides (γ_1 plus γ_2) increase when the catalyst crystal size decreases from conventional to nano-structure catalyst. This is the same order for initial catalyst activity from Figure 1. It should be emphasized that during pretreatment no graphitic carbon is observed. Based on Bartholomew et al. [6,7,19] results, we concluded that carbide γ_1 was attributed to $\acute{\varepsilon}$- $Fe_{2.2}C$ and carbide γ_2 was related to Hägg (χ-$Fe_{2.5}C$) and cementite (θ-Fe_3C) carbides. The calculated amounts of these carbides in Table 4 are similar to XRD results. These results show that α-carbon and transformation of α-carbons to carbide that enhanced the catalyst crystal size are decreased because of increasing CO content on surface of catalyst.

Xu, and Bartholomew [19] showed that the C_α/C_β ratio are dependent on H_2 content on surface of catalyst and this ratio enhances while H_2 content increases. Previous results [28] show that when the catalyst crystal size decreases from conventional to nano-structure catalyst, the concentration of the adsorbed hydrogen on the catalyst surface increases, and change of C_α/C_β ratio is in agreement with this fact.

Table 4. Temperature-programmed surface reaction with hydrogen (TPSR-H_2) results of carbonaceous species after pretreatments

Catalyst	Carbidic α		Amorphous β		Carbide γ_1		Carbide γ_2	
	P. T	C. C	P. T	C. C	P. T	C. C	P. T	C. C
Coventional	568	1.1	696	12.2	793	49.9	833	36.8
Nano size	547	3.1	693	15.1	800	55.4	838	26.4

P. T: Peak temperature (K).
C. C: Compositions of carbon species (Mol%).

TPSR-H_2 results for surface carbonaceous species in promoted catalysts after 105 h FTS reaction are shown in Figure 6 and Table 5, respectively. Because of some dramatic effects of the Soxhlet wax extraction on carbonaceous species, which is reported by Xu and Bartholomew [19], dewaxation of catalysts after reaction is not considered. In addition, because of oxidizing atmosphere in the lower part of the catalyst bed, the catalyst located on the top of reactor for this treatment is only considered. These spectra, which were best fitted by five peaks assigned to α, β, γ_1, γ_2 and δ species, are assigned to atomic carbon (carbidic), amorphous surface methyl chains or films, bulk iron carbides and graphitic carbon. The carbon equivalents for α-carbon (the most reactive carbon form) and carbides for the promoted catalysts are similar to pretreatments results but the carbide composition and amounts of graphitic carbon changed. Based on XRD results, γ_1 and γ_2 carbons are attributed to Hägg (χ-$Fe_{2.5}C$) and cementite (θ-Fe_3C) carbides, respectively. This is due to the absence of $\acute{\varepsilon}$-$Fe_{2.2}C$ carbides after FTS reaction. As shown in Figure 6 and Table 5, the γ_2/γ_1 carbons ratio (which is related to cementite θ-Fe_3C carbides/Hägg, χ-$Fe_{2.5}C$ carbides ratio) in

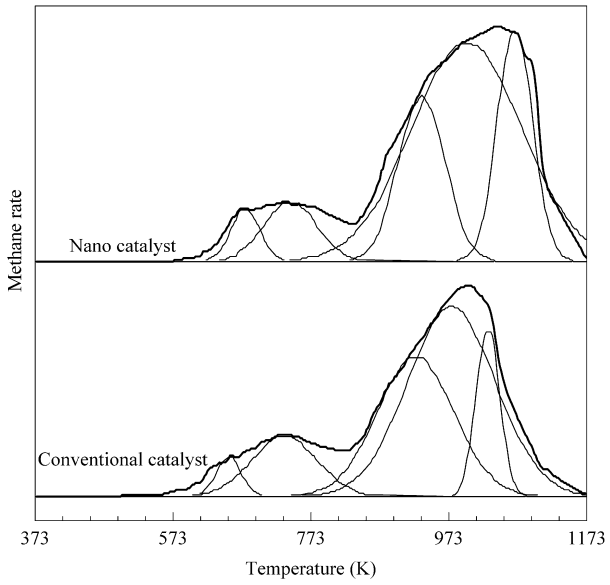

Figure 6. Temperature-programmed surface reaction with hydrogen (TPSR-H_2) of samples after FTS reaction

nano-structure catalyst is higher than conventional catalyst after FTS reaction. Similar results were shown in XRD pattern treatment of used catalysts. This fact is attributed to higher initial activity of this catalyst that enhanced the concentration of oxidizing products (H_2O and CO_2) in reaction atmosphere, and increased the rate of $\acute{\varepsilon}$-$Fe_{2.2}C \rightarrow \chi$-$Fe_{2.5}C \rightarrow \theta$-$Fe_3C$ conversion. It is apparent from Table 5 that amounts of graphitic carbon in used catalysts for nano-structure catalyst are higher than conventional catalyst.

Table 5. Temperature-programmed surface reaction with hydrogen (TPSR-H_2) results of carbonaceous species after 105 h FTS reaction

Catalysts	Carbidic α		Amorphous β		Carbide γ_1		Carbide γ_2		Graphitic δ	
	P. T	C. C	P. T	C. C	P. T	C. C	P. T	C. C	P. T	C. C
Conventional	613	2.7	716	8.6	851	23.1	896	53.0	1000	12.6
Nano size	610	3.1	717	8.5	865	15.9	930	54.0	1005	18.5

P. T: Peak temperature (K);
C. C: Compositions of carbon species (mol%)

4. Discussion

Conventional and nano-structure catalysts were tested in the FTS reaction at 563 K for 105 h. The CO conversions versus time-on-stream for a sample is depicted in Figure 1. The CO conversion improved significantly while the catalyst crystal size decreased. The chemical composition of the sample plays a key role on the catalytic performance. XRD and TPSR-H_2 results indicate that the main iron carbide produced in nano catalysts is $\acute{\varepsilon}$-carbide ($Fe_{2.2}C$). Previous results suggest that the $\acute{\varepsilon}$-carbide ($Fe_{2.2}C$), which produced more than Hägg carbide (χ-$Fe_{2.5}C$) and cementite (θ-Fe_3C) in iron nano-particles after pretreatment, is the most catalytically active phase in FTS reaction [8,9,32]. Also as shown in previous section, the C_α concentration (atomic carbonaceous species resulting from the dissociative adsorption of CO) increased with decreasing crystal size of the iron catalyst.

Xu and Bartholomew [19] concluded that the C_α is the most reactive carbon deposited on the surface of the catalyst. Higher amounts of this species caused higher initial activity of the catalysts after pretreatment. We concluded that the higher initial activity of nano-structure catalyst is attributed to more carbon rich $\acute{\varepsilon}$- $Fe_{2.2}C$ carbides and higher concentration of C_α carbonaceous species.

Deactivation rate of the catalysts is an opposite scenario to the initial catalyst activity. Nano-size iron catalyst has higher deactivation rate and it has been tried to attribute these changes in catalyst activity to variation of catalyst composition.

Eliason and Bartholomew [33] provided evidences that sintering was not responsible for activity loss in iron catalyst. They proposed two deactivation paths while occurring in parallel and/or coupled. In this model, adsorbed α-carbon atoms condensed and polymerized to amorphous β-carbon then to graphitic δ-carbons, and/or in parallel route α-carbon atoms would be precipitated in the transformation of carbon-rich $\acute{\varepsilon}$ to more iron-rich χ and θ phases progressively. These iron carbides transformation increase thermal stability for carbides in the order $\acute{\varepsilon} < \chi < \theta$; presumably Fe–C bond strength increases in the same order. Thus, the activity of iron carbides in hydrogenation of the surface atomic carbon and then FTS activity is in the order $\acute{\varepsilon} > \chi > \theta$ [8,9,32]. Therefore, observed losses of iron catalyst activity are attributed to the transformation of the active carbons into inactive carbons and active carbides into lower active carbides. XRD patterns and TPSR-H_2 results for used catalysts show that nano-structure catalyst has higher amounts of more iron rich cementite (θ-Fe_3C) and inactive graphite-type species that are thermodynamically stable under oxidizing atmosphere in FTS reaction. Based on Bartholomew et al. results [7,19], the deactivation of these catalysts is attributed to two paths: condensation of adsorbed α-carbon atoms to amorphous β-carbon then to graphitic δ-carbons, and/or in parallel route α-carbon atoms would be precipitated in the transformation of carbon-rich $\acute{\varepsilon}$ to more iron-rich χ and θ phases progressively. But the amount of the graphite-type species observed in TPSR-H_2 is higher than our expectation. It has been concluded that another route exists in production of graphite-type species. Jung and Thomson [34] speculated that carbon atoms precipitated by the $\acute{\varepsilon}$ to χ transformation might serve nucleation sites for Boudouard (Eq. 4) reaction.

$$2CO \rightarrow CO_2 + C_s \quad (6)$$

The Reitmeier et al. [35] calculation shows that the main contributor to carbon deposition is CO disproportionation. Then it has proposed another deactivation path for the activity loss of iron catalyst in FTS reaction occurring in parallel with the other two paths. Thus it is concluded that the deactivation of the catalysts occurs in three paths: first, condensation of adsorbed α-carbon atoms to amorphous β-carbon then to graphitic δ-carbons; second, in parallel route, α-carbon atoms would be precipitated in the transformation of carbon-rich $\acute{\varepsilon}$ to more iron-rich χ and θ phases progressively; and third, graphite-type species is produced from CO disproportionation.

5. Conclusions

Decreasing the cluster size of precipitated Fe/Cu/La catalyst into nano scale has been shown to have significant influences on surface carbonaceous species and bulk iron carbides formed in the iron catalysts under Fischer-Tropsch synthesis (FTS) conditions. Bulk iron phase compositions and phase transformations of carbonaceous species during pretreatment and following reaction were characterized us-

ing temperature-programmed surface reaction with hydrogen (TPSR-H_2) and XRD techniques. These results indicate that content of carbon rich $\acute{\varepsilon}$-carbides and C_α carbons (atomic carbonaceous species) after pretreatment were enhanced in nano size iron catalyst. Higher initial activity of nano-structure catalyst was attributed to more carbon rich $\acute{\varepsilon}$- $Fe_{2.2}C$ carbides and higher concentration of C_α carbonaceous species. Both the XRD patterns and TPSR-H_2 results for used catalysts show that nano catalyst have higher amounts of iron rich cementite (θ-Fe_3C) and inactive graphite-type species and that these phases are stable thermodynamically under reducing atmosphere in FTS reaction. Graphite-type species are produced from CO disproportionation and carbon condensation.

References

[1] Anderson R B. The Fischer-Tropsch Synthesis. Orlando, FL: Academic Press, 1984.
[2] Dry M E. In: Anderson J R, Boudart M. ed. Catalysis- Science and Technology. New York: Springer-Verlag, 1981. 159
[3] Bartholomew C H. *Stud Surf Sci Catal*, 1991, 64: 158
[4] van der Laan G P, Beenackers A A C M. *Catal Rev-Sci Eng*, 1999, 41(3-4): 255
[5] Farrauto R J, Bartholomew C H. Introduction to Industrial Catalytic Processes. Chapman & Hall, London: Fundamentals and Practice, 1997, Chap. 6
[6] Eliason S A, Bartholomew C H. *Stud Surf Sci Catal*, 1997, 111: 517
[7] Eliason S A, Bartholomew C H. *Appl Catal A*, 1999, 186(1-2): 229
[8] Pour A N, Shahri S M K, Zamani Y, Irani M, Tehrani S. *J Natur Gas Chem*, 2008, 17(3): 242
[9] Amelse J A, Butt J B, Schwartz L H. *J Phys Chem*, 1978, 82(5): 558
[10] Riedel T, Schulz H, Schaub G, Jun K W, Hwang J S, Lee K W. *Top Catal*, 2003, 26(1-4): 41
[11] Sarkar A, Seth D, Dozier A K, Neathery J K, Hamdeh H H, Davis B H. *Catal Lett*, 2007, 117(1-2): 1
[12] Emmett P H. Catalysis, Vol 4. New York: Reinhold, 1956. 407
[13] Herranz T, Rojas S, Perez-Alonso F J, Ojeda M, Terreros P, Fierro J L G. *J Catal*, 2006, 243(1): 199
[14] Ning W, Koizumi N, Chang H, Mochizuki T, Itoh T, Yamada M. *Appl Catal A*, 2006, 312: 35
[15] Li S, O'Brien R J, Meitzner G D, Hamdeh H, Davis B H, Iglesia E. *Appl Catal A*, 2001, 219(1-2): 215
[16] Niemantsverdriet J W, van der Kraan A M, van Dijk W L, van der Baan H S. *J Phys Chem*, 1980, 84(25): 3363
[17] Dwyer D J, Hardenbergh J H. *J Catal*, 1984, 87(1): 66
[18] Loaiza-Gil A, Fontal B, Rueda F, Mendialdua J, Casanova R. *Appl Catal A*, 1999, 177(2): 193
[19] Xu J, Bartholomew C H. *J Phys Chem B*, 2005, 109(6): 2392
[20] Pour A N, Shahri S M K, Bozorgzadeh H R, Zamani Y, Tavasoli A, Marvast M A. *Appl Catal A*, 2008, 348(2): 201
[21] Pour A N, Housaindokht M R, Tayyari S F, Alaei M R. *J Nat Gas Sci Eng*, in Press, doi:10.1016/j.jngse.2010.02.004
[22] Hayashi H, Chen L Z, Tago T, Kishida M, Wakabayashi K. *Appl Catal A*, 2002, 231(1-2): 81
[23] Li X, Zhong B, Peng S, Wang Q. *Catal Lett*, 1994, 23(3-4): 245
[24] Herranz T, Rojas S, Perez-Alonso F J, Ojeda M, Terreros P, Fierro J L G. *Appl Catal A*, 2006, 311: 66
[25] Eriksson S, Nylen U, Rojas S, Boutonnet M. *Appl Catal A*, 2004, 265(2): 207
[26] Schwuger M J, Stickdorn K, Schomaecker R. *Chem Rev*, 1995, 95(4): 849
[27] Liu C, Zou B, Rondinone A J, Zhang Z J. *J Phys Chem B*, 2000, 104(6): 1141
[28] Pour A N, Taghipoor S, Shekarriz M, Shahri S M K, Zamani Y. *J Nanosci Nanotechno*, 2009, 9(7): 4425
[29] Pour A N, Housaindokht M R, Tayyari S F, Zarkesh J. *J Nat Gas Chem*, in Press, doi: 10.1016/s1003-9953(09)60059-1
[30] Shroff M D, Datye A K. *Catal Lett*, 1996, 37(1-2): 101
[31] Li S, Li A, Krishnamoorthy S, Iglesia E. *Catal Lett*, 2001, 77(4): 197
[32] Obermyer R T, Mulay L N, Lo C, Oskooie-Tabrizi M, Rao V U S. *J Appl Phys*, 1982, 53(3, Pt. 2): 2683
[33] Eliason S A, Bartholomew C H. *Stud Surf Sci Catal*, 1991, 68: 211
[34] Jung H, Thomson W J. *J Catal*, 1992, 134(2): 654
[35] Reitmeier R E, Atwood K, Bennet H A, Baugh H M. *Ind Eng Chem*, 1948, 40(4): 620